Chemistry and Materials Research
ISSN 2224- 3224 (Print) ISSN 2225- 0956 (Online)
Vol.3 No.4, 2013

Synthesis, Characterization and Effect of γ-Ray on Rare-Earth Tb^{3+} Doped Nano Lithium Manganates ($LiMn_{2-x}Tb_xO_4$)

Morsi M. Abou-Sekkina[1] Abdalla M. Khedr[1] Fouad G. El-Metwaly*[1,2]

1. Chemistry Department, Faculty of Science, Tanta University, Tanta - Egypt
2. Chemistry Department, Faculty of Science, Jazan University, Jazan – KSA

* E-mail of the corresponding author: fouadmandoor@yahoo.com

A b s t r a c t

Pure nano lithium manganese oxide spinel ($LiMn_2O_4$) and Tb^{3+} doped lithium manganese oxide spinels [$LiMn_2$-$xTbxO_4$, (x = 0.01%, 0.02%)] are synthesized via solid-state method. The synthesized $LiMn_{1.99}Tb_{0.01}O_4$ was irradiated by γ-irradiation with 30 kGy. The resulting spinel product is characterized by various methods such as thermo gravimetric and differential thermal analysis (TG/DTA), infrared (IR) spectroscopy, x-ray diffraction (XRD), scanning electron microscopy (SEM), energy-dispersive of x-rays analysis (EDAX), electron spin resonances (ESR) studies and DC–electrical conductivity measurements. The XRD and SEM confirm the nano materials size for all prepared samples. DC–electrical conductivity measurements indicates that these samples are semiconductor and the activation energy decreases with increasing rare-earth Tb^{3+} content; ΔE_a = 0.427 eV for $LiMn_{1.99}Tb_{0.01}O_4$, ΔE_a = 0.339 eV for $LiMn_{1.98}Tb_{0.02}O_4$ and decreases to ΔE_a = 0.330 eV for γ-irradiation of $LiMn_{1.99}Tb_{0.01}O_4$ nano spinel thus in role increases its attractiveness in modern electronic technology. Abou-Sekkina activation energy for the induced γ-irradiation is evaluated for the first time, which was found to be 0.097 eV.

Keywords: Nano lithium manganates, Tb^{3+} doping spinel, γ –Ray effect

1. Introduction

Nano lithium manganates ($LiMn_2O_4$) spinels are an attractive candidate, that required to power portable electronic devices (cell phones, laptop computers, etc.). It store electricity from renewable sources, and as a vital component in new hybrid electric vehicles due to their high electromotive force and high energy density [1–2]. $LiMn_2O_4$ spinel is preferable positive electrode (cathodes) of rechargeable lithium ion batteries due to its low cost, non-toxic nature, efficient, environmental friendly and ease of preparation when compared with other layered oxides used for rechargeable lithium ion batteries such as lithium cobalt oxide ($LiCoO_2$) and lithium nickel oxide ($LiNiO_2$) [3–5]. $LiCoO_2$ has many disadvantages such as high cost, toxicity, a negative environmental impact and a low practical specific capacity against its theoretical value. More recently there are reports by several authors that the capacity of pure spinel $LiMn_2O_4$ diminishes at high reduction levels [6, 7]. The capacity fading is due to various factors such as Jahn–Teller distortion (change of a cubic symmetry in to tetragonal one, a two-phase unstable reaction), slow dissolution of manganese into the electrolyte [8], lattice instability [9], and particle-size distribution [10, 11].To suppress the Jahn–Teller distortion and obtain high cycling capacity, many researchers have studied Li-Mn-O spinels in order to improve cyclability by partially chemical substitution of Mn^{3+} with various divalent, trivalent and tetravalent-doped cations such as Co, Zn, Ca, Fe, Ni, Cd, Ga, Ti, and Al [12,13]. Ohuzuku *et al.* [10] and Lee *et al.* [14], have reported that partial doping of divalent and trivalent cations is more effective in suppressing the capacity fade during cycling. The substitution increases the average oxidation state of Mn above 3.5, hence suppressing Jahn-Teller distortion, this lead to stabilize the crystal structure of spinel. All doping elements are less or close to that of Mn, little report about rare-earth elements. So, in our work we concerned on doping of $LiMn_2O_4$ spinel with the rear-earth element Tb^{3+}.

2. Experimental

2.1. Materials Preparation

Nano $LiMn_{2-x}Tb_xO_4$ (x = 0.01%, 0.02%) samples were synthesized by the solid state reaction. Stoichiometric amount of ($LiOH.H_2O$, 99%), manganese carbonate (99.5%) in addition to cautions-doped compounds were mixed and ground thoroughly, pre-sintered at 600°C for 4 hr., then they were reground and pressed in to pellets, sintered in air at 850°C for 8 hr. with a heating rate of 10°C/min. After sintering, cooling with a possible lowest rate, 5°C/min. The prepared spinel materials were identified by x-ray diffraction.

2.2. Instruments and Characterization

The crystal structure of the prepared samples was all analyzed by a Phillips (Holland) x-ray diffractometer (PW 1729 x-ray generator, PW 1840 diffractometer, control, PM 8203 A one line recorder) using Cu Kα radiation (λ = 1.54056 Å) operating at 40.0 kV, 30.0 mA and the datum were collected in the 10–80° 2θ range. The morphology of the products was investigated by scanning electron microscopy (SEM, JSM- 5300LV, Japan) with gold coating and the disppowder was visualized by energy dispersive analysis of X-ray (EDAX). The infrared spectra were recorded using a Perkin–Elmer 1430 IR spectrophotometer within the range 1000-200 cm^{-1} for all samples as KBr discs. Room temperature x-band powder electron spin resonance spectra of the complexes were recorded using a Jeol spectrometer model JES-FE2XG equipped with an E101 microwave bridge using DPPH as reference. The thermal gravimetric analysis (TGA) was carried out in a dynamic nitrogen atmosphere (20 ml min^{-1}) with a heating rate of 10°C min^{-1} using a Shimadzu TG-50 thermogravimetric analyzer. DTA of green samples (uncalcined) were recorded by a Du Pont instruments 990 thermal analyzer (England) of 1200° DTA cell in air at a rate of 10°C min^{-1} at Central Laboratory, Tanta University. The irradiated samples were exposed to γ-irradiation of 30 KGy with dose rate 3.52 KGy/hr at Atomic Energy Authority –National Center for Radiation Research and Technology by Indian gamma source, Nasser city, Cairo. DC-electrical conductivity for all synthesized samples sintered at 850°C for 8 hr. was measured using the two terminal DC-electrical conductivity method, where the pellets of the samples were coated with silver paste, inserted between the two copper probe of the circuit using (Akeithly 175 multimeter USA). This was done at the temperature range from room temperature up to 350°C. The temperature was measured by a calibrated chromel-alumel thermocouple placed firmly at the sample during measurements.

3. Results and Discussion

3.1. Thermal Studies

Fig. 1 represents TGA /DTA curves of the precursor prepared by solid state to prepare doped nano $LiMn_{1.98}Tb_{0.02}O_4$ spinel. In TGA curve, 5% weight loss gradually due to moisture in addition losing H as a result of decomposition LiOH to Li_2O in the range from 65 to 291°C. There is weak endothermic peak at 63 °C due to departure of the adsorbed water in DTA curve. In the second step the weight loss of 22.5% in the range of 291–665°C attributed to medium sharp exothermic peak at 419°C in DTA due to the combustion of residual organic constituents and the loss of oxygen successive phases transfer steps to reach the most stable spinel phase at 850°C.

3.2. X–Ray Diffraction Studies

The Cu–K_α x-ray Powder diffraction (XRD) patterns of the synthesized, pure and doped spinel with different content of Tb^{3+} are shown in Fig. 2. It can be seen from the patterns, all diffraction peaks are very strong which donates the samples have good cubic crystal structure of spinel made of regular tetrahedron [LiO_4] and regular octahedron [MnO_6].

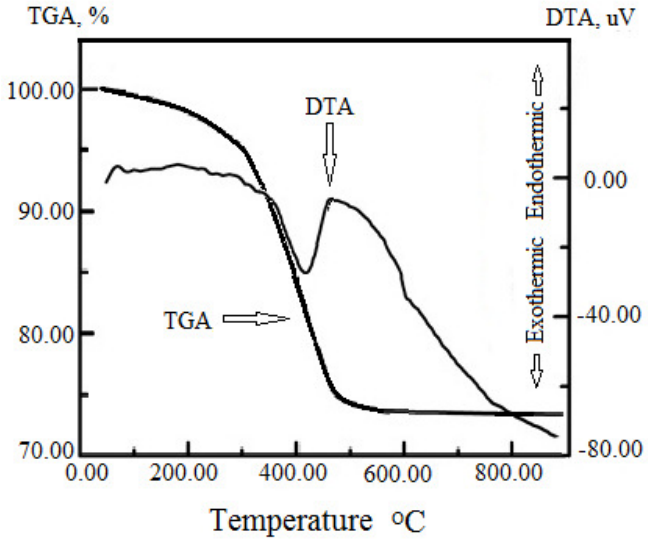

Fig. 1. TGA/DTA curves of the precursor that fired to donate $LiMn_{198}Tb_{0.02}O_4$ nano spinel.

The lattice constant and crystal volume of Tb^{3+} doped spinel bigger than pure one and these are increases with increasing dopant contents, the radius of the sixth coordination Tb^{3+} (0.928 Å), bigger than the radius of Mn^{3+} (0.66 Å). This emphasizes that Tb^{3+} locates the position of Mn^{3+} in MnO_6 octahedral site in the lattic. The XRD after γ-irradiation with 30 kGy is shown in Fig. 3. It can be seen from the patterns that all diffraction peaks are very strong, indicating that the samples have good cubic crystal structure of spinel put the peaks shifted to lower angle, so the lattice constant and crystal volume of γ-irradiation *via* 30 kGy increase than non γ-irradiation sample.

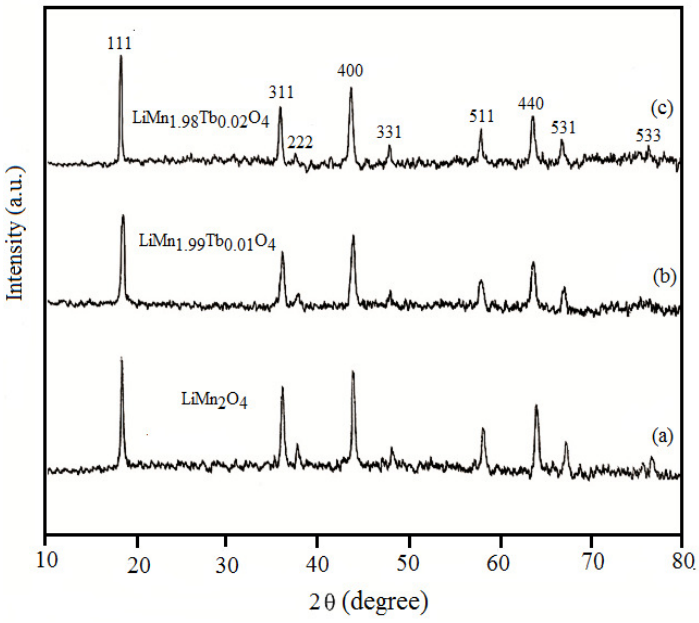

Fig. 2. X-ray diffraction patterns of undoped and doped nano Li-Mn-O spinels ($LiMn_{2-2X}Tb_XO_4$).

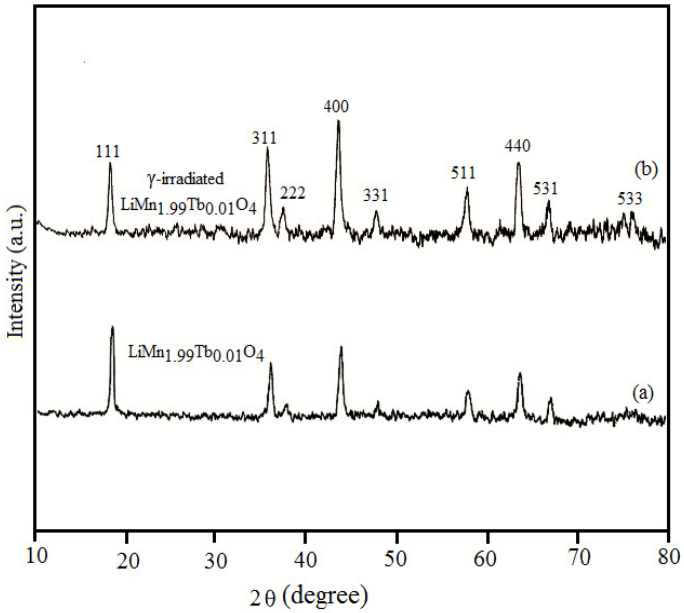

Fig. 3. X-ray diffraction patterns of $LiMn_{1.99}Tb_{0.01}O_4$ nano spinels. (**a**) Non irradiated $LiMn_{1.99}Tb_{0.01}O_4$ spinel and (**b**) $LiMn_{1.99}Tb_{0.01}O_4$ spinel irradiated by 30 kGy.

Table 1. Unit cell parameters and crystallite size of $LiMn_2O_4$, $LiMn_{1.99}Tb_{0.01}O_4$ and $LiMn_{1.98}Tb_{0.02}O_4$ spinels.

No	Sample	a (Å)	Unit cell Volume ($Å^3$)	Crystallite Size x 10^{-9} nm
1	$LiMn_2O_4$	8.186	547	18.97
2	$LiMn_{1.99}Tb_{0.01}O_4$	8.264	564	11.38
3	$LiMn_{1.98}Tb_{0.02}O_4$	8.310	573	18.95
4	$LiMn_{1.99}Tb_{0.01}O_4$ γ-irradiated with 30 kGy	8.329	577	12.44

3.3. IR spectral Studies

Fig. 4 shows The room temperature IR absorption spectra of pure nano $LiMn_2O_4$ spinel by KBr disc technique, which was prepared by solid state method sintered at 850°C for 8 hours, the strong absorption bands at 220, 513 and 613 cm^{-1} are assigned to vibration modes of MnO_6 octahedron. Whereas the band at 260 cm^{-1} is attributable to mixed character of octahedral MnO_6 and LiO_4 tetrahedral building the cubic lattice of nano $LiMn_2O_4$. The obtained infrared spectra of the lattice vibration reveal broad and interfered peaks, where the structure of $LiMn_2O_4$ exhibits a charge disproportion such as $LiMn^{3+}Mn^{4+}O_4$. There are isotropic $Mn^{4+}O_6$ octahedron and locally distorted $Mn^{3+}O_6$ octahedron due to the Jahn-Teller effect. Thus, we expect to observe stretching vibration of $Mn^{4+}O_6$ and $Mn^{3+}O_6$ octahedron which provides a shoulder broad peak at about 518 cm^{-1} of υ_{as} (Mn–O) mode. In the low frequency region, the IR bands at 221 and 260 cm^{-1} have mixed character due to the presence of the bending modes of O–Mn–O bands and modes of LiO_4 group leading to the interference between peaks.

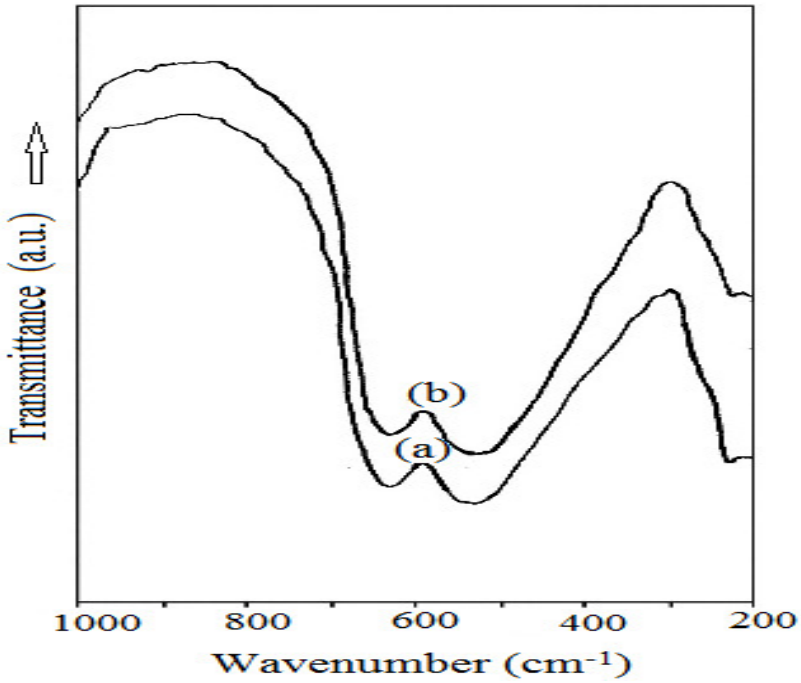

Fig. 4. IR spectra of undoped and doped Li-Mn-O spinels ($LiMn_{2-x}Tb_xO_4$) fired at 850°C in air for 8 h. (**a**) Undoped $LiMn_2O_4$ spinel and (**b**) $_X$ = 0.02% Tb^{3+}.

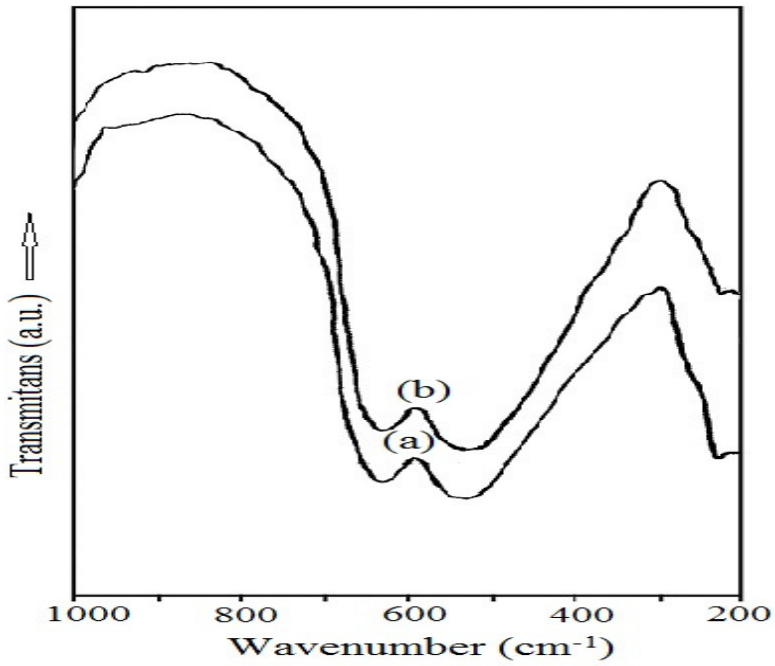

Fig. 5. IR spectra of $LiMn_{1.99}Tb_{0.01}O_4$ spinels. (**a**) Non irradiated $LiMn_{1.99}Tb_{0.01}O_4$ spinel and (**b**) $LiMn_{1.99}Tb_{0.01}O_4$ spinel irradiated with 30 kGy.

This is a characteristic spectrum of $LiMn_2O_4$ spinel in agreement with *C.M. Julien et al.* [16], and *C.Wu et al.* [17]. In conclusion, the spectral features of the LiO_4 remains in the 350–450 cm^{-1} and the vibrational modes of the MnO_6 expand over 450–650 cm^{-1} in addition to the bending modes in 200–350 cm^{-1}. So, the two bands at about 518 and 617 cm^{-1} are spectral feature of cubic nano $LiMn_2O_4$ spinel. The IR spectrum of Tb^{3+} doped spinel consists of overlapped peaks characteristic for Li–Mn–O spinel. The main bands red shift from 518 to 515 and from 617 cm^{-1} to 615 this is for nano $LiMn_{1.99}Tb_{0.01}O_4$ spinel. For nano $LiMn_{1.98}Tb_{0.02}O_4$, the peaks at 221, 518 and 617 are red shifted to 219, 514 and 615 cm^{-1}, respectively. This is an indication for the partial substitution of Mn^{3+} with Tb^{3+} in octahedral position (site). The IR spectra of nano $LiMn_{1.99}Tb_{0.01}O_4$ spinel doped with Tb^{3+} it observed in Fig. 5 which indicates that the γ-irradiated sample have the same spinel cubic structure and the same modes of vibration but peaks at 515, 615 cm^{-1} blue shifted to 518 and 616 cm^{-1} respectively and. These IR spectra give an elucidation the formation of cubic nano pure and doped lithium manganese oxide spinel.

3.4 . SEM and EDAX Analysis

The morphology of powdered samples for pure and doped sample fired at 850°C in air for 8 hr., were investigated by scanning electron microscope (SEM) after coating with gold. Fig. 6 represents the observed images for pure $LiMn_2O_4$, singly doped $LiMn_{1.99}Tb_{0.01}O_4$, $LiMn_{1.98}Tb_{0.02}O_4$ and $LiMn_{1.99}Tb_{0.01}O_4$ spinel irradiated by 30 KGy. These images reveals that the powder exhibits *nano* crystals and this agree with the calculated values of crystal size from x-ray pattern using Scherer's equation, as illustrated in Table 1. The images reveals irregular porous morphology this porous morphology is beneficial for the diffusion of electrolyte into the interior of the particle during fabrication of the battery. Fig. 7 represents the EDAX profile of nano $LiMn_{1.98}Tb_{0.02}O_4$ spinel. This profile of the reflections corresponding to the constituent elements of prepared sample, thus agree with that published by M. Helan *et al.* [18], L. Xiong *et al.* [19] and Thirunakaran *et al.* [20, 21].

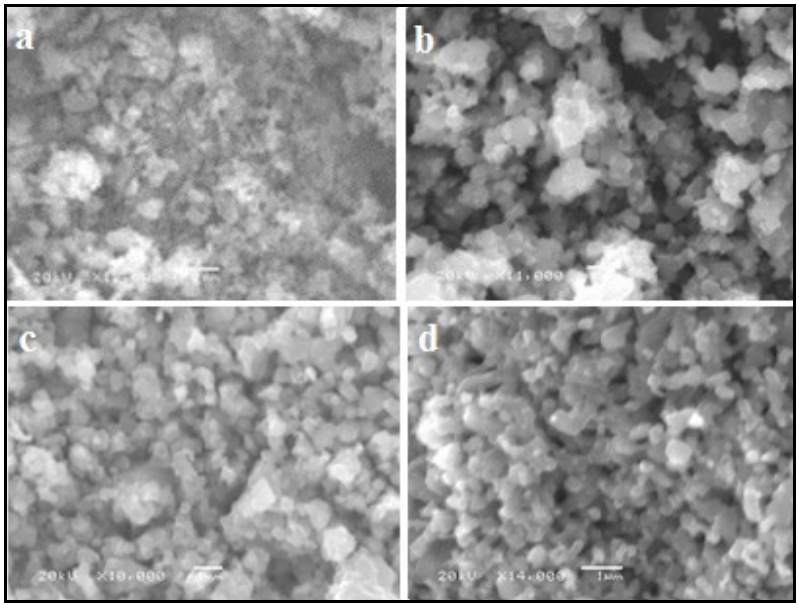

Fig. 6. SEM images of $LiMn_{2-2X}Ag_XY_XO_4$ spinels. (**a**) $LiMn_2O_4$, (**b**) $LiMn_{1.99}Tb_{0.01}O_4$, (**c**) $LiMn_{1.98}Tb_{0.02}O_4$ and (**d**) $LiMn_{1.99}Tb_{0.01}O_4$ spinel irradiated with 30 kGy.

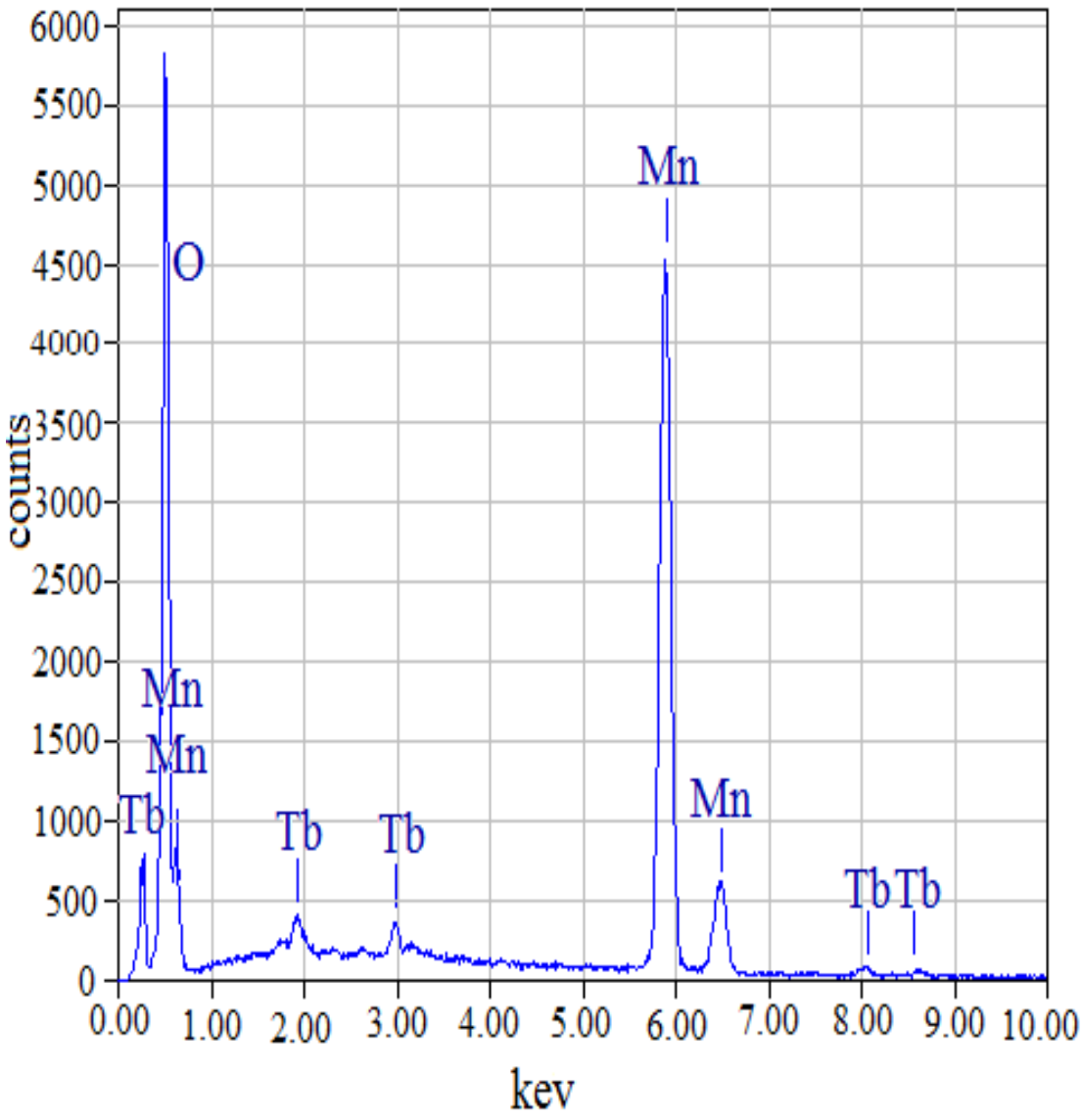

Fig. 7. EDAX profile of nano $LiMn_{1.98}Tb_{0.02}O_4$ spinel.

3.5. ESR Analysis

The paramagnetic behavior of the synthesized crystals is determined using ESR studies. Fig. 8 shows the ESR spectrum of the nano compound. From the figure it is noticed that the paramagnetic character, the spectrum reveals ESR signal attributed to Mn^{3+} ions centered at 3330 G and the corresponding value of g factor is 1.986, which is in good agreement with the reported value for $LiMn_2O_4$. The lone pair electron state is identified from the ESR spectrum. The signal is attributed to Mn^{3+} ions, which are responsible for the paramagnetic entities exist in the compound. Also the ESR signal corresponds to the collective motion of the total magnetic moment of Mn^{3+} and Mn^{4+} spinle systems and this agrees with M. Helan *et al*. [18].

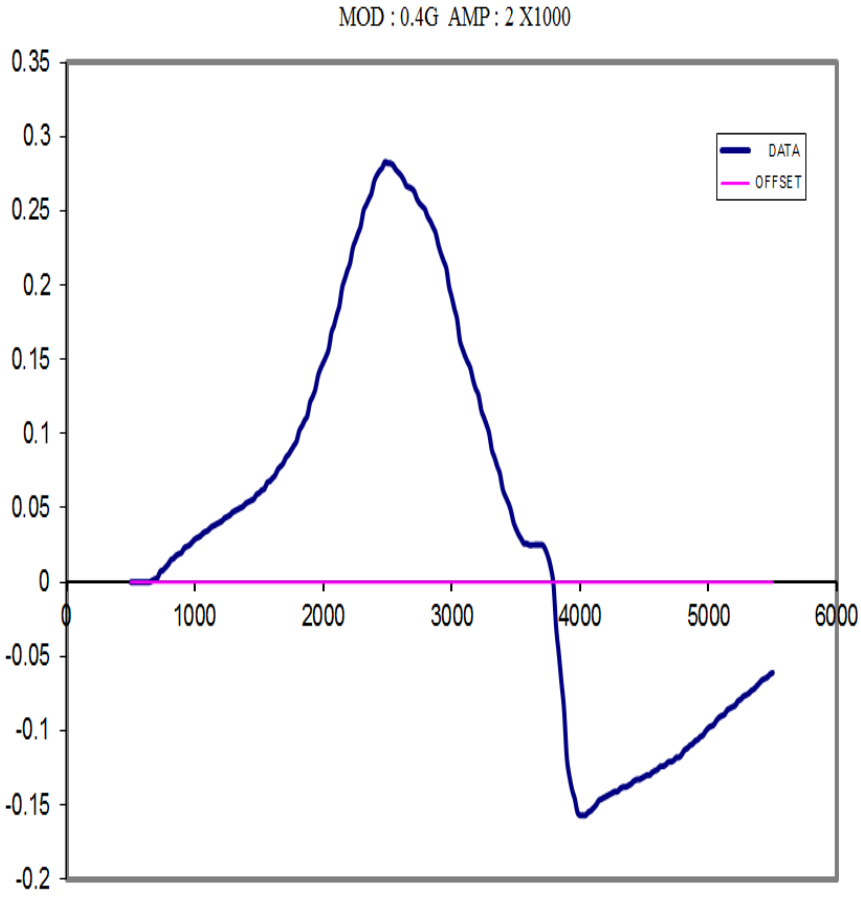

Fig. 8. ESR spectrum of nano $LiMn_{1.98}Tb_{0.02}O_4$ spinel.

3.6. DC–Electrical Conductivity Measurements

The DC–electrical conductivity (lnσ) of various samples has been measured as a function of reciprocal of the absolute temperature (1000/T) K^{-1} from room temperature up to 450°C. According the Arrhenius plot of conductivity corresponding to the relation $\sigma = \sigma_\circ e^{-\Delta Ea/KT}$, where σ is the electrical conductivity $\sigma_\circ$ is the pre-exponential factor, K is the Boltzmann's constant 8.61 X 10^{-5} eV K^{-1}, T is the absolute temperature, ΔE_a is the activation energy for electric conduction[22]. It observed that the conductivity increase with increasing temperature as in Fig. 9 Which indicates semi-conducting behavior for non-irradiated and γ-irradiation samples. These observation can be explained on the basis conduction in $LiMn_2O_4$ nano spinel occurring via small-polaron hopping between $Mn^{3+}$and Mn^{4+}, i.e., unpaired electrons from the e_g orbitals of high spin Mn^{3+} (d_4) hop to neighboring low-spin Mn^{4+} (d_3) ions. Both the e_g orbitals of metal ion lie on the same octahedral site so these are equivalent in energy [23].These samples behaves as extrinsic semiconductor in the range 21–370°C with activation energy ΔE_a = 0.427 eV for $LiMn_{1.99}Tb_{0.01}O_4$, and activation energy reduces for $LiMn_{1.98}Tb_{0.02}O_4$ to ΔE_a = 0.339 eV with increasing dopant content thus as shows by Fig. 10. The ΔE_a =0.330 eV corresponds to irradiated $LiMn_{1.99}Tb_{0.01}O_4$ nano spinel. So, it clear that γ-ray irradiation reduces the activation energy of conduction of the prepared nano samples. Abou-Sekkina activation energy for γ-induced irradiation is depicted to be 0.097 eV.

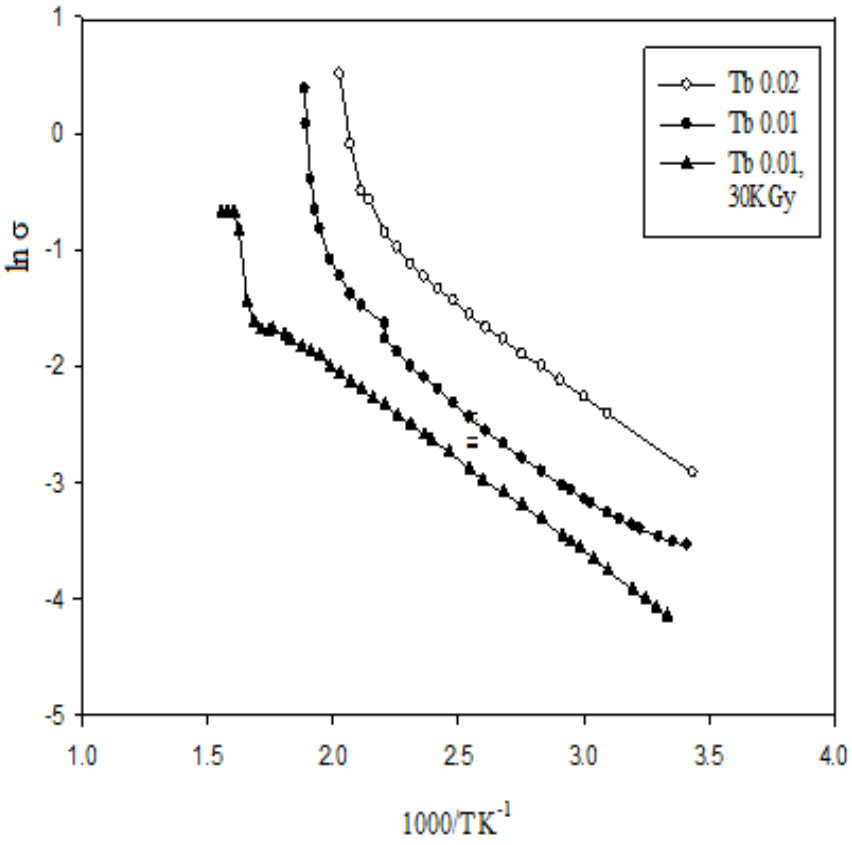

Fig. 9. The variation of DC-electrical conductivity (lnσ) versus reciprocal of absolute temperature (1000/T K^{-1}) for $LiMn_{2-x}Tb_xO_4$ nano spinels. (**a**) $LiMn_{1.99}Tb_{0.01}O_4$, (**b**) $LiMn_{1.98}Tb_{0.02}O_4$ and (**c**) $LiMn_{1.99}Tb_{0.01}O_4$ irradiated with 30 kGy of γ-irradiation.

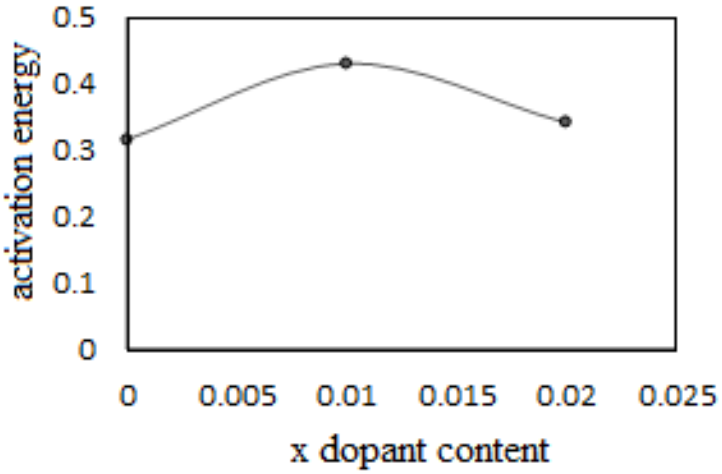

Fig. 10. The variation of activation energy of $LiMn_{2-x}Tb_xO_4$ versus increasing Tb^{3+} content.

4. Conclusion

Pure nano $LiMn_2O_4$, rare-earth Tb^{3+} doped lithium manganese oxide spinel [$LiMn_{2-x}Tb_xO_4$, (x = 0.01%, 0.02 %)], non irradiated and irradiated γ-ray samples are synthesized via solid-state method. The x–ray diffraction data reveals the formation of single-phase spinel with cubic crystal structure for all samples. Also, the x–ray diffraction calculation and SEM images indicated that the prepared spinels are nano compounds with porous morphology of nano crystals within 11-19 nm range. The electrical studies indicate that Tb^{3+} doped to lithium manganese oxide spinel and also, γ-ray irradiation improves its electrical properties. The method used for preparation has a great potential for the commercial preparation of pure $LiMn_2O_4$ and doped $LiMn_{2-x}Tb_xO_4$ spinels. Abou-Sekkina activation energy for the induced γ-irradiation is evaluated for the first time, which was found to be 0.097 eV.

References

[1] Tarascon, J.M. & Armand, M. (2001), "Issues and Challenges Facing Rechargeable Lithium Batteries'', *Nature* **414**, 359-369.

[2] Bruce, P.G., Scrosati, B. & Tarascon, J.M. (2008), "Nanomaterials for Rechargeable Lithium Batteries, *Angewandte Chemie International Edition* **47**, 2930-2946.

[3] Tarascon, J.M., McKinnon, W.R., Coowar, F., Bowner, T.N., Amatucci, G. & Guyomard, D.J. (1994), "Synthesis Condition and Oxygen Stoichiometry Effect on Li Insertion in to the Spinele $LiMn_2O_4$" *Journal of Electrochemical Society* **141**, 1421-1431.

[4] Gummow, R.J., de Kock, A. & Thackeray, M.M. (1994), "Improved Capacity Retention in Rechargeable 4 V Lithium/Lithium-Manganes Oxide (Spinel) Cells", *Solid State Ionics* **69**, 59-67.

[5] Thackeray, M.M., de Kock, A., Rossouw, M.H., Liles, D., Bittihn, R. & Hoge, D.J. (1992), "Spinel Electrodes from the Li-Mn-O System for Rechargeable Lithium Battery Applications", *Journal of Electrochemical Society* **139**, 363-366.

[6] Xia, Y. & Yoshio, M. (1997), "Optimization of Spinel $Li_{1+x}Mn_{2-y}O_4$ as a 4 V Li-Cell Cathode in Terms of a Li-Mn-O Phase Diagram", *Journal of Electrochemical Society* **144**, 4186-4194.

[7] Pistoia, G., Antonini, A., Rosati, R. & Zane, D.J. (1996), "Storage Characteristics of Cathodes for Li-ion Batteries", *Electrochemical Acta* **41**, 2673-2689.

[8] Jang, D.H., Shin, J. & Oh, S.M. (1996), "Dissolution of Spinel Oxides and Capacity Losses in 4 V $Li / Li_xMn_2O_4$ Cells", *Journal of Electrochemical Society* **143**, 2204-2211.

[9] Yamada, A. (1996), "Lattice Instability in $Li(Li_xMn_{2-x})O_4$", *Journal of Solid State Chemistry* **122**, 160-165.

[10] Ohuzuku, T., Takeda, S. & Iwanaga, M. (1999), "Olivine Coated Spinel : 5V Systemfor High Energy Lithium Batteries", *Journal of Power Sources* **90**, 81-82.

[11] Song, D., Ikuta, H., Uchida, T. & Wakihara, M. (1999), "The Spinel Phases $LiAl_yMn_{2-y}O_4$ (y=0, 1/12, 1/9, 1/6, 1/3) and $Li(Al,M)_{1/6}Mn_{11/6}O_4$ (M=Cr, Co) as the Cathode for Rechargeable Lithium Batteries, *Solid State Ionics* **117**, 151-156.

[12] JavedIqbal, M. & Zahoor, S. (2007), "Synthesis and Characterization of Nanosized Lithium Manganate and its Derivatives", *Journal of Power Sources* **165**, 393-397.

[13] Kumar, G., Schlorb, H. & Rahner, D. (2001), "Synthesis and Electrochemical Characterization of 4 V $LiR_XMn_{2-X}O_4$ Spinels for Rechargeable Lithium Batteries", *Materials Chemistry and* Physics **70**, 117-123.

[14] Lee, J.H., Hong, J.K., Jang, D.H., Sun, Y.K. & Oh, S.M. (2000). "Degradation Mechanisms in Doped Spinels of $LiM_{0.05}Mn_{1.95}O_4$ (M = Li, B, Al,Co, and Ni) for Li Secondary Batteries", *Journal of Power Sources* **89**, 7-14.

[15] Tu, J., Zhao, X.B., Cao, G.S., Zhu, T.J & Tu, J.P. (2006), "Enhanced Cycling Stability of $LiMn_2O_4$ by Surface Modification with Melting Impregnation Method", *Electrochemical Acta* **51**, 6456–6462.

[16] Julien, C.M. & Mussot (2003), "Lattice Vibrations of Materials for Lithium Rechargeable Oxide Spinel", *Materials Science and Engineering B* **97**, 217-230.

[17] Wu, C., Wang, Z., Wu, F., Chen, L. & Hang, X. (2000), "Spectroscopic Studies on Cation-doped Spinel $LiMn_2O_4$ for Lithium Ion Batteries", *Solid State Ionics* **144**, 277-285.

[18] Helan, M;, Berchman, L., Jose, T., Visuvasam, A. & Angappan, S. (2010), "Molten Salt Synthesis of $LiMn_2O_4$ Using Chloride–Carbonate Melt", *Materials Chemistry and Physics* **124**, 439-442.

[19] Xiong, L., Xu, Y., Tao, T. & Goodenough, J.B. (2012), "Synthesis and Electrochemical Characterization of Multi-Cations Doped Spinel $LiMn_2O_4$ used for Lithium Ion Batteries", *Journal of Power Sources* **199**, 214-217.

[20] Thirunakaran, R., Sivashanmugam, A., Gopukumar, S., & Rajalakshmi, R. (2009) "Cerium and zinc: Dual-doped $LiMn_2O_4$ spinels as cathode material for use in lithium rechargeable batteries", *Journal of Power Sources* **187**, 565-574.

[21] Thirunakaran, R., Ravikumar, R., Gopukumar, S. & Sivashanmugam, A. (2013), "Electrochemical Evaluation of Dual-doped $LiMn_2O_4$ Spinels Synthesized via Co-Precipitation Method as Cathode Material For Lithium Rechargeable Batteries", *Journal of Alloys and Compounds* **556**, 266-273.

[22] Raman, R., Murthy, V.R.K. & Viswanathan, B.J. (1991), "Microwave Dielectric Loss Studies on Lithium - Zinc Ferrites", *Applied Physics A* **69**, 4053-4055.

[23] Vitioo I., PhD Thesis, (1999), "Synthesis, structure, conductivity and electrode properties for some double disulphates, silicates and lithium manganese oxide", University of Latvia.